Journal of Sound and Vibration 330 (2011) 1153–1165

Contents lists available at ScienceDirect

Journal of Sound and Vibration

journal homepage: www.elsevier.com/locate/jsvi

An analytical study of sound transmission through unbounded panels of functionally graded materials

Changzheng Huang*, Steven Nutt [1]

Department of Chemical Engineering and Materials Science, University of Southern California, Los Angeles, CA 90089-0241, USA

ARTICLE INFO

Article history:
Received 2 June 2010
Accepted 22 September 2010
Handling Editor: Y. Auregan
Available online 15 October 2010

ABSTRACT

The problem of sound transmission and reflection from unbounded panels of functionally graded materials is studied using an analytical approach. By means of matrix manipulation and Fourier component analysis, the three-dimensional (3-D) governing equations of elastodynamics are converted into a system of ordinary differential equations with variable coefficients in the frequency and wavenumber domain. Integration of the ordinary differential equation system across the panel thickness leads to a closed-form solution for the transfer matrix. Analytical expressions are then obtained for sound reflection and transmission coefficients for panels of functionally graded materials. The present model is used to predict sound transmission losses for various panel examples. The results compare well with published data from other methods, thereby validating the accuracy of the formulation developed in this study.

1. Introduction

The interaction between an acoustic wave and a panel structure is an important subject that arises from practical applications. Panel structures are often used to build walls and other structural components of vehicles and airplanes. These structural panels are intended to not only withstand various internal and external loads, but also to provide acoustic insulation from the noisy environment. Therefore, analysis and optimization of the acoustic characteristics of panels is an integral part of the design of airframe structures [1]. Acoustic waveforms, after interacting with panel structures, may be modified in a way specific to the panel geometry, underlying defects, and material compositions. Therefore, acoustic signals reflected or transmitted from panel structures carry useful information that can be used for acoustic imaging [2], non-destructive evaluation [3], structural health monitoring [4], and estimation of material properties [5,6]. In this work, we mainly focus on an analytical study of sound transmission and reflection from panels of functionally graded materials (FGM).

Functionally graded panels are structures made of two or more materials in which the volume fraction of each component varies continuously in the thickness direction, thereby achieving some desired function. Vibration and wave propagation in functionally graded panels has been studied numerically and analytically. For example, Liu et al. did some classical work on characteristics of surface waves on functionally graded piezoelectric material plates [7]. Chakraborty and Gopalakrishnan [8] studied wave propagation in functionally graded materials using a variant of the finite element method called the spectral layer element. This element is exact if the material properties follow an exponential relationship across the panel thickness. Reddy [9] developed finite element models based on the third-order shear deformation plate theory for the analysis of through-thickness functionally graded plates. Venkataraman and Sankar [10] obtained an elasticity

* Corresponding author. Tel.: +12137408929.
E-mail addresses: changzh@usc.edu (C. Huang), nutt@usc.edu (S. Nutt).
[1] Tel.: +12137401634.

0022-460X/$ - see front matter © 2010 Elsevier Ltd. All rights reserved.
doi:10.1016/j.jsv.2010.09.020

solution for stresses in a sandwich beam with functionally graded core. Vel and Batra [11] obtained an exact solution for three-dimensional deformations of a simply supported functionally graded rectangular plates subjected to mechanical and thermal loads on its surfaces. Wang and Rokhlin [12] derived differential equations governing transfer and stiffness matrices for wave propagation in a functionally graded multi-layered elastic medium. Shuvalov et al. [13] considered propagation of guided acoustic waves in infinite functionally graded piezoelectric plates using the state-vector formalism.

In contrast, the literature on sound transmission through functionally graded panels is relatively scarce. Hasheminejad and Shabanimotlagh [14] focused on this topic, and reported their numerical work on sound insulation characteristics of functionally graded panels. On the other hand, studies on the sound transmission through multi-layered panels, particularly through sandwich panels, have been extensive [15–24]. For example, Thomson applied the classical method of transfer matrix to study transmission of elastic waves through a stratified solid medium [15]. Smolenski and Krokosky [16] focused on the dilational-mode sound transmission in sandwich panels. Guyader and Lesueur [17] studied acoustic transmission through orthotropic multi-layered plates using a numerical approach. Dym and Lang [18] considered transmission loss of damped asymmetric sandwich panels with orthotropic cores. Wang et al. [19] used a higher-order method to predict sound transmission, while Assaf and Guerich [20] applied the finite element method to study noise transmission loss through viscoelastically damped sandwich plates. In recent years, analytical method that is based on the exact stress–strain relationship has gained some popularity [21–24]. With this analytical approach, Cai et al. analyzed sound reflection and transmission for anisotropic laminates and other paneled structures [21,22]. Lin et al. [23] obtained sound transmission loss across specially orthotropic laminates. Based on 3-D elasticity theory, Huang and Nutt [24] developed analytical formulations for sound transmission and reflection from multi-layered panels.

In this study, we extend our prior work based on 3-D elasticity theory to develop analytical formulations for acoustic reflection and transmission from unbounded panels of functionally graded materials. In the frequency and wavenumber domain, the governing elastodynamics equations are converted into a system of first-order ordinary differential equations with variable coefficients for functionally graded panels, in which the material properties vary only in the thickness direction. Similar procedure was also used in prior studies known as propagator matrix method [25,26] or state-space method [21,22]. We solved the variable coefficient equation system by performing a matrix exponential to derive the transfer matrix and then obtained the analytical solutions for sound transmission and reflection coefficients. The resulting analytical expressions are applicable to both FGM panels and multi-layered panels. In fact, our formulation can be viewed as a unified treatment for these two panel types. In the following account, we first develop the modeling theory, then present examples and results to validate the formulation.

2. Theory

In this section, we will develop the analytical formulation for sound transmission and reflection from infinite panels comprised of functionally graded materials (FGM). We first consider the panel dynamics in the physical space-time domain, then derive the transfer matrix in the spectral and wavenumber domain, and finally solve for the transmission and reflection coefficients.

2.1. Panel dynamics in physical domain

The interaction between an incident acoustic wave and an infinite FGM panel of thickness h is shown schematically in Fig. 1. The plane acoustic wave impinges on one surface of the FGM panel with an incident angle θ. As a result, a reflected wave and a transmitted wave are generated from the incident (bottom) and exit (top) surfaces of the panel, respectively.

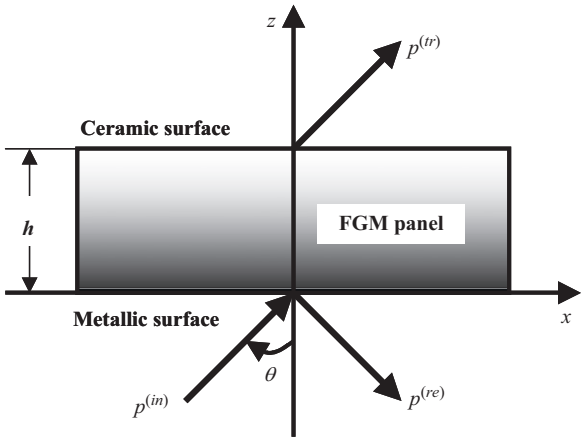

Fig. 1. An incident sound wave $p^{(in)}$ impinges on the bottom surface of an FGM panel with an incident angle θ, which is then split into a reflected wave $p^{(re)}$ from the bottom surface and a transmitted wave $p^{(tr)}$ from the top surface. The incident wave lies in the xz-plane, which makes the azimuthal angle $\phi=0$.

The panel dynamics in the physical domain is described by the elastodynamics equations,

$$\begin{aligned}\frac{\partial\sigma_{xx}}{\partial x}+\frac{\partial\sigma_{yx}}{\partial y}+\frac{\partial\sigma_{zx}}{\partial z}&=\rho\frac{\partial^2 u}{\partial t^2},\\ \frac{\partial\sigma_{xy}}{\partial x}+\frac{\partial\sigma_{yy}}{\partial y}+\frac{\partial\sigma_{zy}}{\partial z}&=\rho\frac{\partial^2 v}{\partial t^2},\\ \frac{\partial\sigma_{xz}}{\partial x}+\frac{\partial\sigma_{yz}}{\partial y}+\frac{\partial\sigma_{zz}}{\partial z}&=\rho\frac{\partial^2 w}{\partial t^2}.\end{aligned} \tag{1}$$

where ρ is the density of the panel, and

$$\begin{aligned}\mathbf{u}&=(u,v,w)^{\mathrm{T}},\\ \boldsymbol{\sigma}&=(\sigma_{xx},\sigma_{yy},\sigma_{zz},\sigma_{yz},\sigma_{zx},\sigma_{xy})^{\mathrm{T}}\end{aligned} \tag{2}$$

are column vectors of the displacement and stresses, respectively. Here, the symmetric property of the stress tensor is assumed, i.e., $\boldsymbol{\sigma}_{ij}=\boldsymbol{\sigma}_{ji}$. Consider a transversely isotropic FGM panel whose mechanical properties (density and elastic moduli) vary in the panel thickness direction, i.e., the z-direction, but not in the in-plane (x,y)-directions. Note that the displacement and the z-component stresses are continuous in the thickness direction because these stress components are the normal components to the inhomogeneity, that is

$$\begin{pmatrix}u\\ v\\ w\end{pmatrix}_{z^-}=\begin{pmatrix}u\\ v\\ w\end{pmatrix}_{z^+}, \tag{3}$$

$$\begin{pmatrix}\sigma_{zx}\\ \sigma_{zy}\\ \sigma_{zz}\end{pmatrix}_{z^-}=\begin{pmatrix}\sigma_{zx}\\ \sigma_{zy}\\ \sigma_{zz}\end{pmatrix}_{z^+}. \tag{4}$$

The equation above suggests that the stress vector $\boldsymbol{\sigma}$ can be re-grouped into two sub-vectors, i.e., a z-component sub-vector and an in-plane component sub-vector

$$\boldsymbol{\sigma}_1'=\begin{pmatrix}\sigma_{zx}\\ \sigma_{zy}\\ \sigma_{zz}\end{pmatrix},\quad \boldsymbol{\sigma}_2'=\begin{pmatrix}\sigma_{xx}\\ \sigma_{yy}\\ \sigma_{xy}\end{pmatrix}. \tag{5}$$

In lieu of re-grouping the stress vector, Eq. (1) can be re-written as

$$\begin{pmatrix}0&0&0\\0&0&0\\1&0&0\end{pmatrix}\frac{\partial}{\partial x}\begin{pmatrix}\sigma_{zx}\\ \sigma_{zy}\\ \sigma_{zz}\end{pmatrix}+\begin{pmatrix}0&0&0\\0&0&0\\0&1&0\end{pmatrix}\frac{\partial}{\partial y}\begin{pmatrix}\sigma_{zx}\\ \sigma_{zy}\\ \sigma_{zz}\end{pmatrix}+\frac{\partial}{\partial z}\begin{pmatrix}\sigma_{zx}\\ \sigma_{zy}\\ \sigma_{zz}\end{pmatrix}+\begin{pmatrix}1&0&0\\0&0&1\\0&0&0\end{pmatrix}\frac{\partial}{\partial x}\begin{pmatrix}\sigma_{xx}\\ \sigma_{yy}\\ \sigma_{xy}\end{pmatrix}+\begin{pmatrix}0&0&1\\0&1&0\\0&0&0\end{pmatrix}\frac{\partial}{\partial y}\begin{pmatrix}\sigma_{xx}\\ \sigma_{yy}\\ \sigma_{xy}\end{pmatrix}=\rho\frac{\partial^2}{\partial t^2}\begin{pmatrix}u\\ v\\ w\end{pmatrix}. \tag{6}$$

We next turn to the strain–stress relationship and make it consistent with the re-grouping Eq. (5). The general strain–stress relationship for a structural element is

$$\boldsymbol{\varepsilon}=\begin{pmatrix}\varepsilon_{xx}\\ \varepsilon_{yy}\\ \varepsilon_{zz}\\ \varepsilon_{yz}\\ \varepsilon_{zx}\\ \varepsilon_{xy}\end{pmatrix}=\begin{pmatrix}S_{11}&S_{12}&S_{13}&S_{14}&S_{15}&S_{16}\\ S_{21}&S_{22}&S_{23}&S_{24}&S_{25}&S_{26}\\ S_{31}&S_{32}&S_{33}&S_{34}&S_{35}&S_{36}\\ S_{41}&S_{42}&S_{43}&S_{44}&S_{45}&S_{46}\\ S_{51}&S_{52}&S_{53}&S_{54}&S_{55}&S_{56}\\ S_{61}&S_{62}&S_{63}&S_{64}&S_{65}&S_{66}\end{pmatrix}\begin{pmatrix}\sigma_{xx}\\ \sigma_{yy}\\ \sigma_{zz}\\ \sigma_{yz}\\ \sigma_{zx}\\ \sigma_{xy}\end{pmatrix}=\mathbf{S}\boldsymbol{\sigma}, \tag{7}$$

where $\boldsymbol{\varepsilon}$ is the strain vector and $\mathbf{S}$ the compliance matrix. Recall that for an orthotropic FGM panel, the mechanical properties change in the thickness direction. Therefore, the compliance matrix $\mathbf{S}$ in Eq. (7) is a function of z, i.e.

$$\mathbf{S}=\mathbf{S}(z). \tag{8}$$

As mentioned earlier, we shall reorganize the stress vector into two parts, i.e., a z-component part and an in-plane component part

$$\boldsymbol{\sigma}=\begin{pmatrix}\sigma_{xx}\\ \sigma_{yy}\\ \sigma_{zz}\\ \sigma_{yz}\\ \sigma_{zx}\\ \sigma_{xy}\end{pmatrix}=\begin{pmatrix}\begin{pmatrix}0&0&0\\0&0&0\\0&0&1\end{pmatrix}&\begin{pmatrix}1&0&0\\0&1&0\\0&0&0\end{pmatrix}\\ \begin{pmatrix}0&1&0\\1&0&0\\0&0&0\end{pmatrix}&\begin{pmatrix}0&0&0\\0&0&0\\0&0&1\end{pmatrix}\end{pmatrix}\begin{pmatrix}\begin{pmatrix}\sigma_{zx}\\ \sigma_{zy}\\ \sigma_{zz}\end{pmatrix}\\ \begin{pmatrix}\sigma_{xx}\\ \sigma_{yy}\\ \sigma_{xy}\end{pmatrix}\end{pmatrix}=\begin{pmatrix}\mathbf{M}_{11}&\mathbf{M}_{12}\\ \mathbf{M}_{21}&\mathbf{M}_{22}\end{pmatrix}\begin{pmatrix}\boldsymbol{\sigma}_1'\\ \boldsymbol{\sigma}_2'\end{pmatrix}=\mathbf{M}\boldsymbol{\sigma}'. \tag{9}$$

Next we re-arrange the strain vector in similar fashion

$$\boldsymbol{\varepsilon}=\begin{pmatrix}\varepsilon_{xx}\\ \varepsilon_{yy}\\ \varepsilon_{zz}\\ \varepsilon_{yz}\\ \varepsilon_{zx}\\ \varepsilon_{xy}\end{pmatrix}=\begin{pmatrix}\begin{pmatrix}0&0&0\\0&0&0\\0&0&1\end{pmatrix} & \begin{pmatrix}1&0&0\\0&1&0\\0&0&0\end{pmatrix}\\ \begin{pmatrix}0&1&0\\1&0&0\\0&0&0\end{pmatrix} & \begin{pmatrix}0&0&0\\0&0&0\\0&0&1\end{pmatrix}\end{pmatrix}\begin{pmatrix}\begin{pmatrix}\varepsilon_{zx}\\ \varepsilon_{zy}\\ \varepsilon_{zz}\end{pmatrix}\\ \begin{pmatrix}\varepsilon_{xx}\\ \varepsilon_{yy}\\ \varepsilon_{xy}\end{pmatrix}\end{pmatrix}=\begin{pmatrix}\mathbf{M}_{11}&\mathbf{M}_{12}\\ \mathbf{M}_{21}&\mathbf{M}_{22}\end{pmatrix}\begin{pmatrix}\boldsymbol{\varepsilon}'_1\\ \boldsymbol{\varepsilon}'_2\end{pmatrix}=\mathbf{M}\boldsymbol{\varepsilon}'. \tag{10}$$

Substitution of Eqs. (9) and (10) into Eq. (7) yields

$$\boldsymbol{\varepsilon}'=\mathbf{M}^{-1}\mathbf{S}\mathbf{M}\boldsymbol{\sigma}'=\mathbf{S}'\boldsymbol{\sigma}'. \tag{11}$$

This equation can be written explicitly as

$$\boldsymbol{\varepsilon}'=\begin{pmatrix}\boldsymbol{\varepsilon}'_1\\ \boldsymbol{\varepsilon}'_2\end{pmatrix}=\begin{pmatrix}\begin{pmatrix}\varepsilon_{zx}\\ \varepsilon_{zy}\\ \varepsilon_{zz}\end{pmatrix}\\ \begin{pmatrix}\varepsilon_{xx}\\ \varepsilon_{yy}\\ \varepsilon_{xy}\end{pmatrix}\end{pmatrix}=\begin{pmatrix}\begin{pmatrix}\partial w/\partial x+\partial u/\partial z\\ \partial w/\partial y+\partial v/\partial z\\ \partial w/\partial z\end{pmatrix}\\ \begin{pmatrix}\partial u/\partial x\\ \partial v/\partial y\\ \partial v/\partial x+\partial u/\partial y\end{pmatrix}\end{pmatrix}=\begin{pmatrix}\mathbf{S}'_{11}&\mathbf{S}'_{12}\\ \mathbf{S}'_{21}&\mathbf{S}'_{22}\end{pmatrix}\begin{pmatrix}\boldsymbol{\sigma}'_1\\ \boldsymbol{\sigma}'_2\end{pmatrix}. \tag{12}$$

Eq. (12) can be re-written as two equations—one for the z-component strain, and one for the in-plane strain

$$\begin{pmatrix}0&0&1\\0&0&0\\0&0&0\end{pmatrix}\frac{\partial}{\partial x}\begin{pmatrix}u\\ v\\ w\end{pmatrix}+\begin{pmatrix}0&0&0\\0&0&1\\0&0&0\end{pmatrix}\frac{\partial}{\partial y}\begin{pmatrix}u\\ v\\ w\end{pmatrix}+\frac{\partial}{\partial z}\begin{pmatrix}u\\ v\\ w\end{pmatrix}=\mathbf{S}'_{11}\boldsymbol{\sigma}'_1+\mathbf{S}'_{12}\boldsymbol{\sigma}'_2, \tag{13}$$

$$\begin{pmatrix}1&0&0\\0&0&0\\0&1&0\end{pmatrix}\frac{\partial}{\partial x}\begin{pmatrix}u\\ v\\ w\end{pmatrix}+\begin{pmatrix}0&0&0\\0&1&0\\1&0&0\end{pmatrix}\frac{\partial}{\partial y}\begin{pmatrix}u\\ v\\ w\end{pmatrix}=\mathbf{S}'_{21}\boldsymbol{\sigma}'_1+\mathbf{S}'_{22}\boldsymbol{\sigma}'_2. \tag{14}$$

With tensor notation, Eqs. (13) and (14) can be written in a more compact form as

$$\mathbf{N}_{11}\frac{\partial\mathbf{u}}{\partial x}+\mathbf{N}_{12}\frac{\partial\mathbf{u}}{\partial y}+\frac{\partial\mathbf{u}}{\partial z}=\mathbf{S}'_{11}\boldsymbol{\sigma}'_1+\mathbf{S}'_{12}\boldsymbol{\sigma}'_2, \tag{15}$$

$$\mathbf{N}_{21}\frac{\partial\mathbf{u}}{\partial x}+\mathbf{N}_{22}\frac{\partial\mathbf{u}}{\partial y}=\mathbf{S}'_{21}\boldsymbol{\sigma}'_1+\mathbf{S}'_{22}\boldsymbol{\sigma}'_2. \tag{16}$$

Comparing the coefficient matrices in Eq. (6) with those in Eqs. (13) and (14), Eq. (6) can be written as

$$\mathbf{N}_{11}^{\mathrm{T}}\frac{\partial\boldsymbol{\sigma}'_1}{\partial x}+\mathbf{N}_{12}^{\mathrm{T}}\frac{\partial\boldsymbol{\sigma}'_1}{\partial y}+\frac{\partial\boldsymbol{\sigma}'_1}{\partial z}+\mathbf{N}_{21}^{\mathrm{T}}\frac{\partial\boldsymbol{\sigma}'_2}{\partial x}+\mathbf{N}_{22}^{\mathrm{T}}\frac{\partial\boldsymbol{\sigma}'_2}{\partial y}=\rho\frac{\partial^2\mathbf{u}}{\partial t^2}. \tag{17}$$

Eqs. (15)–(17) constitute a system of partial differential equations for three vector variables, $\mathbf{u}$, $\boldsymbol{\sigma}'_1$ and $\boldsymbol{\sigma}'_2$. Note that the variable $\boldsymbol{\sigma}'_2$ does not possess a partial derivative with respect to z, and thus can be eliminated from Eqs. (15) and (17) using Eq. (16). The result is

$$\frac{\partial\mathbf{u}}{\partial z}=-\mathbf{N}_{11}\frac{\partial\mathbf{u}}{\partial x}-\mathbf{N}_{12}\frac{\partial\mathbf{u}}{\partial y}+\mathbf{S}'_{11}\boldsymbol{\sigma}'_1+\mathbf{S}'_{12}(\mathbf{S}'_{22})^{-1}\left(\mathbf{N}_{21}\frac{\partial\mathbf{u}}{\partial x}+\mathbf{N}_{22}\frac{\partial\mathbf{u}}{\partial y}-\mathbf{S}'_{21}\boldsymbol{\sigma}'_1\right), \tag{18}$$

$$\frac{\partial\boldsymbol{\sigma}'_1}{\partial z}=\rho\frac{\partial^2\mathbf{u}}{\partial t^2}-\mathbf{N}_{11}^{\mathrm{T}}\frac{\partial\boldsymbol{\sigma}'_1}{\partial x}-\mathbf{N}_{12}^{\mathrm{T}}\frac{\partial\boldsymbol{\sigma}'_1}{\partial y}-\left(\mathbf{N}_{21}^{\mathrm{T}}\frac{\partial}{\partial x}+\mathbf{N}_{22}^{\mathrm{T}}\frac{\partial}{\partial y}\right)(\mathbf{S}'_{22})^{-1}\left(\mathbf{N}_{21}\frac{\partial\mathbf{u}}{\partial x}+\mathbf{N}_{22}\frac{\partial\mathbf{u}}{\partial x}-\mathbf{S}'_{21}\boldsymbol{\sigma}'_1\right). \tag{19}$$

Eqs. (18) and (19) are general, as they are derived from the elastodynamics Eqs. (1) and the constitutive strain–stress relationship in Eq. (7).

2.2. Fourier component analysis and transfer matrix

We will use the method of Fourier component analysis to simplify Eqs. (18) and (19). Because the FGM panels of our interest have infinite extent in the x and y directions, the Fourier component in the frequency and wavenumber domain can be written as

$$\begin{aligned}\mathbf{u}(t,x,y,z)&=\overline{\mathbf{u}}(\omega,k_x,k_y,z)e^{\mathrm{i}k_x x}e^{\mathrm{i}k_y y}e^{-\mathrm{i}\omega t},\\ \boldsymbol{\sigma}'_1(t,x,y,z)&=\overline{\boldsymbol{\sigma}'_1}(\omega,k_x,k_y,z)e^{\mathrm{i}k_x x}e^{\mathrm{i}k_y y}e^{-\mathrm{i}\omega t},\end{aligned} \tag{20}$$

where k_x and k_y are wavenumbers in the x and y directions, respectively, and ω is the circular frequency. Substitution of Eq. (20) into Eqs. (18) and (19) yields a system of first-order ordinary differential equations in terms of the over-barred variables

$$\frac{d}{dz}\begin{pmatrix}\overline{\mathbf{u}}\\ \overline{\boldsymbol{\sigma}}_1'\end{pmatrix}=\begin{pmatrix}\mathbf{A}_{11} & \mathbf{A}_{12}\\ \mathbf{A}_{21} & \mathbf{A}_{22}\end{pmatrix}\begin{pmatrix}\overline{\mathbf{u}}\\ \overline{\boldsymbol{\sigma}}_1'\end{pmatrix}. \tag{21}$$

Referring to Eqs. (18) and (19), we have

$$\mathbf{A}_{11}=-(\mathrm{i}k_x\mathbf{N}_{11}+\mathrm{i}k_y\mathbf{N}_{12})+\mathbf{S}_{12}'(\mathbf{S}_{22}')^{-1}(\mathrm{i}k_x\mathbf{N}_{21}+\mathrm{i}k_y\mathbf{N}_{22}), \tag{22}$$

$$\mathbf{A}_{12}=\mathbf{S}_{11}'-\mathbf{S}_{12}'(\mathbf{S}_{22}')^{-1}\mathbf{S}_{21}', \tag{23}$$

$$\mathbf{A}_{21}=\rho(-\mathrm{i}\omega)^2-(\mathrm{i}k_x\mathbf{N}_{21}^{\mathrm{T}}+\mathrm{i}k_y\mathbf{N}_{22}^{\mathrm{T}})(\mathbf{S}_{22}')^{-1}(\mathrm{i}k_x\mathbf{N}_{21}+\mathrm{i}k_y\mathbf{N}_{22}), \tag{24}$$

$$\mathbf{A}_{22}=-(\mathrm{i}k_x\mathbf{N}_{11}^{\mathrm{T}}+\mathrm{i}k_y\mathbf{N}_{12}^{\mathrm{T}})+(\mathrm{i}k_x\mathbf{N}_{21}^{\mathrm{T}}+\mathrm{i}k_y\mathbf{N}_{22}^{\mathrm{T}})(\mathbf{S}_{22}')^{-1}\mathbf{S}_{21}'. \tag{25}$$

Recall from Eq. (8) that the compliance matrix $\mathbf{S}$ is a function of z. Therefore Eq. (21) is an ordinary differential equation with variable coefficient matrix, i.e.

$$\frac{d\boldsymbol{\psi}}{dz}=\mathbf{A}(z)\boldsymbol{\psi}. \tag{26}$$

Here

$$\boldsymbol{\psi}=\begin{pmatrix}\overline{\mathbf{u}}\\ \overline{\boldsymbol{\sigma}}_1'\end{pmatrix}. \tag{27}$$

The solution for Eq. (26) can be written as

$$\boldsymbol{\psi}(z)=\left[\exp\int_0^z\mathbf{A}(z)\,dz\right]\boldsymbol{\psi}(0). \tag{28}$$

In particular the solution at the exit (top) surface of the panel, where $z=h$, is

$$\boldsymbol{\psi}(h)=\left[\exp\int_0^h\mathbf{A}(z)\,dz\right]\boldsymbol{\psi}(0)=\mathbf{T}\boldsymbol{\psi}(0). \tag{29}$$

Using Eq. (27), Eq. (29) can be written as

$$\begin{pmatrix}\overline{\mathbf{u}}(h)\\ \overline{\boldsymbol{\sigma}}_1'(h)\end{pmatrix}=\left[\exp\int_0^h\mathbf{A}(z)\,dz\right]\begin{pmatrix}\overline{\mathbf{u}}(0)\\ \overline{\boldsymbol{\sigma}}_1'(0)\end{pmatrix}=\mathbf{T}\begin{pmatrix}\overline{\mathbf{u}}(0)\\ \overline{\boldsymbol{\sigma}}_1'(0)\end{pmatrix}, \tag{30}$$

where $\mathbf{T}$ is the transfer matrix that relates the variables (displacement and z-component stresses) on the incident surface of the panel $z=0$ to those at the exit surface $z=h$. Eq. (30) is one of the key results of this study. The transfer matrix derived here applies not only to functionally graded panels, but also to multi-layered panels. Note for multi-layered panels, the transfer matrix is calculated simply by layer-wise summations over all the layers

$$\mathbf{T}=\exp\int_0^h\mathbf{A}(z)\,dz=\sum_{n=1}^{N}\mathbf{A}_n h_n. \tag{31}$$

Therefore, we have arrived at a unified transfer matrix that is valid for both FGM panels and multi-layered panels. We next make use of this transfer matrix to derive acoustic transmission and reflection coefficients for graded or layered structural panels.

2.3. Acoustic reflection and transmission coefficients

Referring to the diagram in Fig. 1 showing a plane wave incident on an unbounded panel, we can write the incident wave traveling in air as

$$p^{(\mathrm{in})}(x,y,z,t)=e^{\mathrm{i}\mathbf{k}\cdot\mathbf{x}}e^{-\mathrm{i}\omega t}=e^{\mathrm{i}k_x x+\mathrm{i}k_y y+\mathrm{i}k_z z}e^{-\mathrm{i}\omega t}. \tag{32}$$

The wavenumber components must satisfy,

$$k_x^2+k_y^2+k_z^2=k_0^2=\omega^2/c_0^2, \tag{33}$$

where k_0 and c_0 are the wavenumber and speed of sound in the air, respectively. If the incident wave makes a polar angle θ and an azimuthal angle ϕ with respect to the xz-plane, we have

$$k_x=k_0\sin\theta\cos\phi,\quad k_y=k_0\sin\phi,\quad k_z=k_0\cos\theta\cos\phi. \tag{34}$$

Without loss of generality, we assume the wave propagation vector $\mathbf{k}$ is on the xz-plane, which makes the azimuthal angle $\phi=0$. The reflected wave and transmitted wave can be written as

$$p^{(\mathrm{re})}(x,y,z,t)=Re^{\mathrm{i}k_x x+\mathrm{i}k_y y-\mathrm{i}k_z z}e^{-\mathrm{i}\omega t}, \tag{35}$$

$$p^{(\mathrm{tr})}(x,y,z,t) = Te^{\mathrm{i}k_x x + \mathrm{i}k_y y + \mathrm{i}k_z z}e^{-\mathrm{i}\omega t}, \tag{36}$$

where R and T are the coefficients of the reflected and transmitted pressure waves, respectively. The fluid motion caused by each such wave can be determined from the acoustic equations. The fluid particle displacement in the z-direction can be written as

$$w^{(\mathrm{in})} = \frac{\mathrm{i}k_z}{\rho_0\omega^2}e^{\mathrm{i}k_x x + \mathrm{i}k_y y + \mathrm{i}k_z z}e^{-\mathrm{i}\omega t}, \tag{37}$$

$$w^{(\mathrm{re})} = -\frac{\mathrm{i}k_z}{\rho_0\omega^2}Re^{\mathrm{i}k_x x + \mathrm{i}k_y y - \mathrm{i}k_z z}e^{-\mathrm{i}\omega t}, \tag{38}$$

$$w^{(\mathrm{tr})} = \frac{\mathrm{i}k_z}{\rho_0\omega^2}Te^{\mathrm{i}k_x x + \mathrm{i}k_y y + \mathrm{i}k_z z}e^{-\mathrm{i}\omega t}, \tag{39}$$

where ρ_0 is the air density. The boundary conditions on the top and bottom panel surfaces can be imposed in the frequency and wavenumber domain. The top and bottom panel surfaces are in contact with the acoustic medium air. Therefore, the z-component displacement and normal stress must be continuous, i.e., $w=w^{(\mathrm{air})}$ and $\sigma_{zz}=-p^{(\mathrm{air})}$. In addition, the z-component shear stresses must vanish, i.e., $\sigma_{zx}=\sigma_{zy}=0$. As a result, Eq. (30) becomes

$$\begin{pmatrix} \overline{u}^{(\mathrm{Top})} \\ \overline{v}^{(\mathrm{Top})} \\ \mathrm{i}k_z T'/\rho_0\omega^2 \\ 0 \\ 0 \\ -T' \end{pmatrix} = \begin{pmatrix} t_{11} & t_{12} & t_{13} & t_{14} & t_{15} & t_{16} \\ t_{21} & t_{22} & t_{23} & t_{24} & t_{25} & t_{26} \\ t_{31} & t_{32} & t_{33} & t_{34} & t_{35} & t_{36} \\ t_{41} & t_{42} & t_{43} & t_{44} & t_{45} & t_{46} \\ t_{51} & t_{52} & t_{53} & t_{54} & t_{55} & t_{56} \\ t_{61} & t_{62} & t_{63} & t_{64} & t_{65} & t_{66} \end{pmatrix} \begin{pmatrix} \overline{u}^{(\mathrm{Bot})} \\ \overline{v}^{(\mathrm{Bot})} \\ \mathrm{i}k_z(1-R)/\rho_0\omega^2 \\ 0 \\ 0 \\ -(1+R) \end{pmatrix}, \tag{40}$$

where t_{ij} are entries of the transfer matrix $\mathbf{T}$ as defined in Eq. (30). The superscripts "Top" and "Bot" refer to the top and bottom surface of the panel respectively. T' and T are related by

$$T' = -Te^{\mathrm{i}k_z h}. \tag{41}$$

Note that Eq. (40) constitutes six linear equations for solving six unknown variables. By Cramer's rule, the solution for R and T' is

$$R = \frac{(\mathrm{i}\kappa)M_3 - (\rho_0 c_0\omega)M_6}{(\mathrm{i}\kappa)M_3 + (\rho_0 c_0\omega)M_6}, \tag{42}$$

$$T' = \frac{-2(\mathrm{i}\kappa)(\rho_0 c_0\omega)N}{(\mathrm{i}\kappa)M_3 + (\rho_0 c_0\omega)M_6}, \tag{43}$$

where $\kappa=k_z/k_0$, and

$$M_3 = \begin{vmatrix} t_{31} & t_{32} & t_{33} & \mathrm{i}\kappa \\ t_{41} & t_{42} & t_{43} & 0 \\ t_{51} & t_{52} & t_{53} & 0 \\ t_{61} & t_{62} & t_{63} & -\rho_0 c_0\omega \end{vmatrix}, \tag{44}$$

$$M_6 = \begin{vmatrix} t_{31} & t_{32} & t_{36} & \mathrm{i}\kappa \\ t_{41} & t_{42} & t_{46} & 0 \\ t_{51} & t_{52} & t_{56} & 0 \\ t_{61} & t_{62} & t_{66} & -\rho_0 c_0\omega \end{vmatrix}, \tag{45}$$

$$N = \begin{vmatrix} t_{31} & t_{32} & t_{33} & t_{36} \\ t_{41} & t_{42} & t_{43} & t_{46} \\ t_{51} & t_{52} & t_{53} & t_{56} \\ t_{61} & t_{62} & t_{63} & t_{66} \end{vmatrix}. \tag{46}$$

Using R and T' as determined from Eqs. (42) and (43), the acoustic reflection and transmission coefficients are computed as

$$r = |R|^2, \quad \tau = |T'|^2. \tag{47}$$

The analytical solution for the sound reflection and transmission coefficients as defined in Eqs. (42)–(46) is second key result of this study. As with the transfer matrix in Eq. (30), the acoustic reflection and transmission coefficients are applicable to both functionally graded panels and multi-layered panels. Therefore we have derived a unified formulation for analyzing sound characteristics of panel structures.

2.4. Comparison with conventional formalism

At this point we can compare the current formulation with the conventional approach for dealing with sound transmission through functionally graded panels. In the conventional method [14], an FGM panel is first divided into multiple thin layers. For each thin layer, the mechanical properties are approximated as constant. The acoustic governing equations are then solved by enforcing matching boundary conditions at layer interfaces. In essence, this approach treats an FGM panel as a multi-layered panel. The underlying assumption is that if the number of divided thin layers is sufficiently large, then the staired profile of mechanical properties will approximate the original FGM profile. There are pitfalls associated with this classical approach, as described below.

First, the classical approach does not specify the number of layers in which the panel must be divided. As a result, consequently, one may have to use different numbers of layer divisions to check and ensure convergence of the result. This leads to added complexity and computational inefficiency. On the other hand, the current formulation is naturally suited for dealing with FGM panels while treating multi-layered panels as a special case.

Secondly, because the conventional approach is an approximate method for analyzing an FGM panel, the interpretation of the numerical result is less straightforward, limiting the insight into the effects of some panel parameters. For instance, in the conventional approach, the grazing angle $\theta=90^\circ$ is regarded as a singularity condition because it causes division-by-zero error in the numerical treatment [14]. However, this grazing angle is not an actual singularity, as we can show from the analytical solution. At the grazing angle $\theta=90^\circ$, we have $\kappa=k_z/k_0=\cos\theta=0$. Substituting $\kappa=0$ into Eqs. (42)–(47), we see that $r=1$ and $\tau=0$. In other words, at the grazing angle $\theta=90^\circ$, we get full acoustic reflection and no transmission. This is expected and consistent with intuition. The effect of other panel properties is incorporated in the values of M_3, M_6 and N as defined in Eqs. (44)–(46).

With the analytical solution obtained for FGM panels, we will consider some examples on sound transmission characteristics of panel structures. In the study of sound transmission, the term sound transmission loss (TL) is often used, and it is defined as

$$\mathrm{TL}=10\log_{10}\left(\frac{1}{\tau}\right). \tag{48}$$

If the incident sound field is diffuse in nature, i.e., all incident angles are equally possible, then the averaged transmission coefficient is used, given by

$$\overline{\tau}=\frac{\int_0^{2\pi}\left[\int_0^{\pi/2}\tau(\theta,\phi)\sin\theta\cos\theta\,d\theta\right]d\phi}{\int_0^{2\pi}\left[\int_0^{\pi/2}\sin\theta\cos\theta\,d\theta\right]d\phi}. \tag{49}$$

In the equation above, the averaging is performed over all possible incident angles.

2.5. Evaluation of matrix exponential

Before presenting numerical examples, Eq. (29) warrants further comment. This equation involves the evaluation of the exponential of a matrix,

$$\mathbf{T}=\exp\int_0^h\mathbf{A}(z)\,dz=e^{\mathbf{B}}. \tag{50}$$

Theoretically, if the matrix $\mathbf{B}$ has a full set of eigenvectors $\mathbf{V}$ with corresponding eigenvalues $\mathbf{D}$

$$\mathbf{B}=\mathbf{V}\mathbf{D}\mathbf{V}^{-1}=\mathbf{V}\begin{pmatrix}\lambda_1 & 0 & \cdots & 0\\ 0 & \lambda_2 & & 0\\ \vdots & & \ddots & \vdots\\ 0 & 0 & \cdots & \lambda_n\end{pmatrix}\mathbf{V}^{-1}. \tag{51}$$

Then the exponential of the matrix would be

$$\mathbf{T}=\exp(\mathbf{B})=\mathbf{V}\begin{pmatrix}\exp(\lambda_1) & 0 & \cdots & 0\\ 0 & \exp(\lambda_2) & & 0\\ \vdots & & \ddots & \vdots\\ 0 & 0 & \cdots & \exp(\lambda_n)\end{pmatrix}\mathbf{V}^{-1}. \tag{52}$$

However, direct computation of Eq. (52) may present numerical difficulty. In the numerical examples presented below, we used the MATLAB library function *expm* to evaluate the matrix exponential. This library function employs a scaling and squaring algorithm with a Pade approximation to compute the exponential of a matrix. Interested readers are referred to the paper by Higham [27] for more details on the algorithm. Numerically well-conditioned formulation can also be found in the reference by Liu [28].

3. Results

The current analytical solution applies to functionally graded panels as well as to multi-layered panels. As part of the model validation, we first consider sound transmission through an isotropic aluminum panel and compare the solution with available experimental data. We then apply the analytical solution to various FGM panels and compare the sound transmission predictions with published numerical results. In all the examples below, we assume the panel is in contact with air both at the incident (bottom) and exit (top) half-spaces. The air density is taken to be $\rho_0=1.25$ kg/m^3, and the speed of sound in the air to be $c_0=340$ m/s.

3.1. Single-layer isotropic aluminum panel

This first example is taken from the work of Leppington et al. [29], who studied sound transmission through an aluminum panel (thickness 2.5 mm, density $\rho=2700$ kg/m^3, Young's modulus $E=71$ GPa and Poisson's ratio $\mu=0.33$). In our calculations, we assumed a loss factor of $\eta=0$ for aluminum.

Fig. 2 shows a plot of the transmission coefficient τ as a function of the incident angle θ and the frequency f. Note that for a given frequency, there is one transmission peak in the plot that occurs near the grazing angle $\theta=90^\circ$. For a given frequency greater than the critical frequency (in this case, $f_c=4800$ Hz), there is a second transmission peak $\tau=1$ at a moderate incident angle This second peak is a phenomenon of acoustic coincidence that is caused by the matching of the trace wavenumber in the panel with that in the ambient air [30]. Above the critical frequency, the coincident transmission dominates, while the near-grazing transmission decreases.

When the incident acoustic wave arises from a diffuse sound field, then the measured transmission coefficient is generally an averaged value, as defined in Eq. (49). Fig. 3 shows a comparison between the transmission loss values

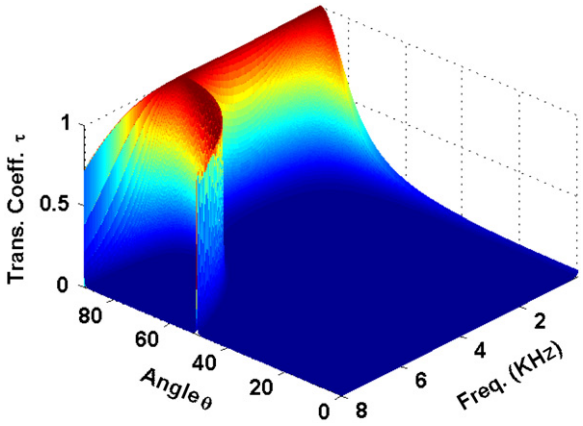

Fig. 2. Plot of the transmission coefficients τ as a function of the incident angle θ and the frequency f for a single-layer aluminum panel.

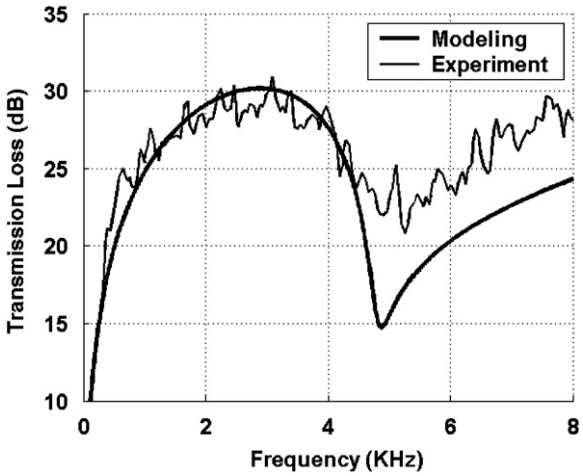

Fig. 3. A comparison of sound transmission loss for an aluminum panel. Thick line is result from present model and thin line is experimental data [29].

generated from model-based predictions with those measured experimentally. The experimental data was obtained from an aluminum panel 1.4 m × 0.9 m. The finite dimensions and boundary constraints of the panel caused resonances or eigen-vibrations in the in-plane directions. These resonances are manifest in the experimental curve as fine-scale oscillations (modal resonance peaks and dips). In contrast, the modeling curve is smooth and void of fine-scale oscillations because the modeled panel was assumed to be infinite in the in-plane directions. The effect of panel size is not the prime concern here, although this issue has been analyzed elsewhere [31].

The plot in Fig. 3 shows that the model accurately predicts the critical coincident frequency at ~4800 Hz. In addition, the agreement between the model prediction and the measured data is good for frequencies less than the coincident frequency. However, for frequencies greater than the coincident frequency, a deviation of about 5 dB is noted between theory and experiment. This discrepancy is attributed to acoustic damping of the material, which plays a more important role above the critical coincident frequency. In our modeling we assumed no damping, i.e., zero loss factor η=0 for the aluminum panel.

3.2. FGM panels

We next consider examples of sound transmission through panels of functionally graded materials (FGM). We begin with a metal–ceramic FGM panel that is purely metallic on one surface and purely ceramic on the opposite. Such FGM panels can carry loads and provide thermal protection. The volume fraction of each component changes smoothly between 0% and 100% in the panel thickness direction. The compositional change can be in a linear or nonlinear fashion. Fig. 4 shows three scenarios for the volume fraction change of the metal in the range of $0 \le z \le h$. We assume the volume variation can be described by a power law function as follows [14]:

$$V_m(z) = \left(1 - \frac{z}{h}\right)^n, \tag{53}$$

where V_m is the volume fraction of metallic constituent. The exponent n can take different values to represent different scenarios, for instance

$$\begin{cases} n = 0.2 & \text{Metal Rich (MR)}, \\ n = 1.0 & \text{Linear (LN)}, \\ n = 5.0 & \text{Ceramic Rich (CR)}. \end{cases} \tag{54}$$

The effective material properties at any location, such as the density ρ, Lame's constants λ and μ, are approximated by a linear combination of those of the individual constituents weighted by the volume fraction of each phase [14], i.e.

$$\begin{aligned} \rho(z) &= V_m\rho_m + V_c\rho_c, \\ \lambda(z) &= V_m\lambda_m + V_c\lambda_c, \\ \mu(z) &= V_m\mu_m + V_c\mu_c, \end{aligned} \tag{55}$$

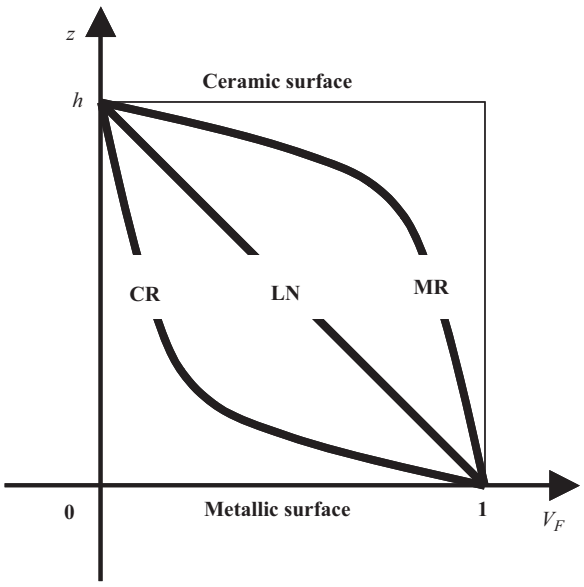

Fig. 4. Three cases of compositional variations in the thickness direction of FGM panel: metal rich (MR), linear (LN), and ceramic rich (CR).

where the subscript m indicates the metal phase and the subscript c indicates the ceramic phase. V_c is the volume fraction of ceramic constituent. The stiffness matrix $\mathbf{C}$ at location z is then given by

$$\mathbf{C}(z)=\begin{pmatrix} \lambda+2\mu & \lambda & \lambda & 0 & 0 & 0 \\ \lambda & \lambda+2\mu & \lambda & 0 & 0 & 0 \\ \lambda & \lambda & \lambda+2\mu & 0 & 0 & 0 \\ 0 & 0 & 0 & \mu & 0 & 0 \\ 0 & 0 & 0 & 0 & \mu & 0 \\ 0 & 0 & 0 & 0 & 0 & \mu \end{pmatrix}. \tag{56}$$

The compliance matrix $\mathbf{S}$ as defined in Eq. (7) is just the inverse of the stiffness matrix $\mathbf{C}$. With this, the transfer matrix $\mathbf{T}$ in Eq. (30), the sound transmission coefficient τ in Eq. (47), and the sound transmission loss TL in Eq. (48) can all be evaluated.

To extend the comparison, two additional FGM panel examples are considered [14]. In the cited work, the authors adopted the conventional approach and divided the FGM panel into multiple discrete layers. Each layer was divided thinly so that the material properties were assumed to possess constant values within the layer. In other words, the FGM panel was essentially treated as a multi-layered panel. In contrast, we employ an analytical formulation for FGM panels. An FGM panel is treated as a single entity without layer division, as evidenced in the transfer matrix definition Eq. (30).

Our first example of an FGM panel is a metal–ceramic panel comprised of stainless steel (SUS304) and silicon nitride (Si_3N_4). The properties of the stainless steel are, density ρ=8166 kg/m^3, Lame's constants λ=179 GPa, and μ=102.7 GPa, while properties for silicon nitride are, density ρ=2370 kg/m^3, Lame's constants λ=119.9 GPa, and μ=129.9 GPa. We computed sound transmission loss for three cases of metal–ceramic compositions, i.e., metal rich (MR), linear (LN), and ceramic rich (CR), as defined in Eqs. (53) and (54). The sound transmission loss is displayed in Fig. 5 as a function of acoustic frequency at four different incident angles, i.e., θ=0°, 30°, 45°, and 75°. Comparison is also made with the available numerical result from the work of Hasheminejad and Shabanimotlagh [14]. For the sake of clarity, comparison is displayed only for the metal-rich panel in the plots. The accuracy of the current formulation is demonstrated by the good agreement between the results from these two different approaches.

The numerical results lead to some direct observations. First, the transmission loss curves for incident angles θ=30°, 45°, and 75° show a large dip in the middle frequency range. This large dip occurs at the critical coincidence frequency f_c. Below f_c, the transmission loss is controlled largely by the mass law, while above f_c, the transmission loss is controlled

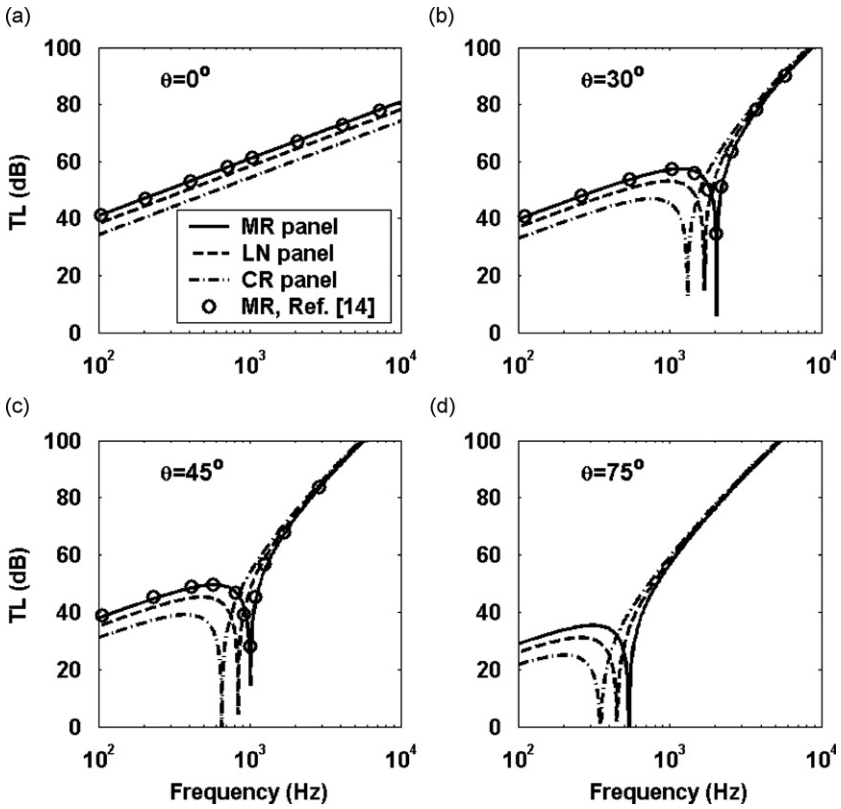

Fig. 5. Transmission loss (TL) as a function of incident wave frequency for a SUS304/Si_3N_4 FGM panel. Three panel cases, i.e., metal rich (MR), linear (LN), and ceramic rich (CR), are plotted, and four incident angles are considered: (a) θ=0°, (b) θ=30°, (c) θ=45°, and (d) θ=75°.

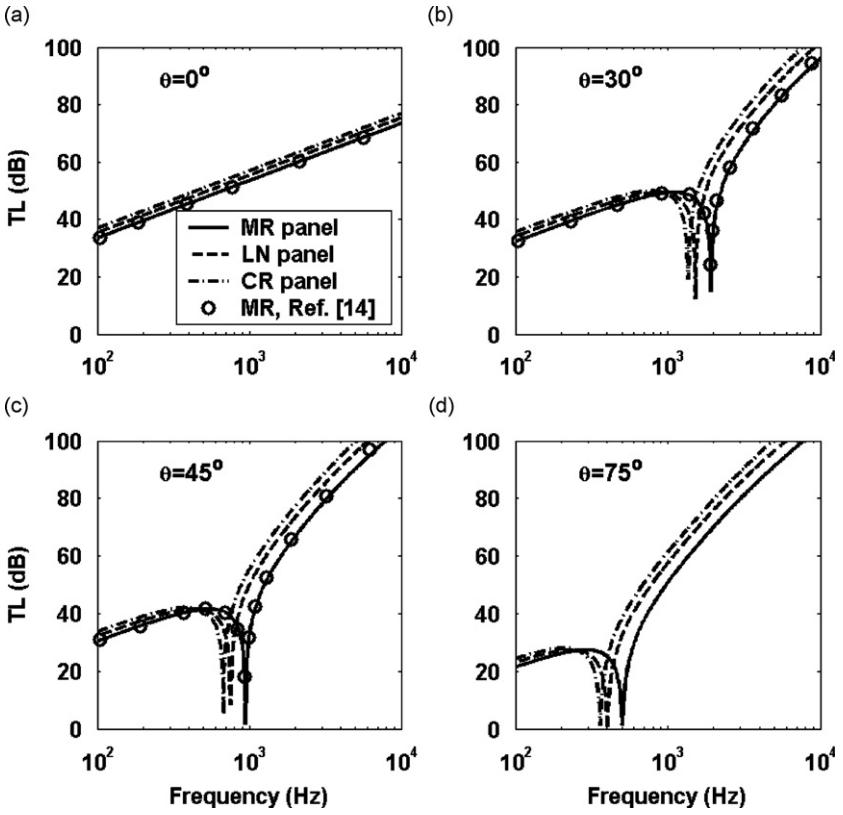

Fig. 6. Transmission loss (TL) as a function of incident wave frequency for a Al/TiC FGM panel. Three panel cases, i.e., metal rich (MR), linear (LN), and ceramic rich (CR), are plotted, and four incident angles are considered: (a) θ=0°, (b) θ=30°, (c) θ=45°, and (d) θ=75°.

mainly by the stiffness of the panel. The transmission loss curve for incident angle θ=0° does not show a large dip in the frequency range from 10 Hz to 10 KHz, indicating an absence of the acoustic coincidence phenomenon at this incident angle. Secondly, the critical coincidence frequency decreases as the incident angle increases. This is true whether the FGM panel is metal rich (MR), linear (LN), or ceramic rich (CR). Thirdly, below the critical coincidence frequency f_c, the transmission loss is largest for the metal-rich panel, and smallest for the ceramic-rich panel. Above the critical coincidence frequency f_c, this trend is reversed, but differences in transmission loss diminish at higher frequencies. This last observation, however, is panel-specific, and cannot be generalized to other metal–ceramic panels. In fact, our next panel example will show the opposite behavior in transmission loss.

Our second example is a metal–ceramic FGM panel comprised of aluminum and titanium carbide (Al/TiC). The properties for aluminum are, density ρ=2700 kg/m^3, Lame's constants λ=50.4 GPa, and μ=25.9 GPa, while those for titanium carbide are, density ρ=4920 kg/m^3, Lame's constants λ=133.3 GPa, and μ=200 GPa. Again, we consider the transmission loss for three cases, i.e., metal-rich, linear and ceramic-rich. The computational results are plotted in Fig. 6. Inspection of these plots shows that the first two observations for the previous panel example also apply to this panel example. That is, the acoustic coincidence phenomenon occurs for incident angles θ=30°, 45°, and 75°, but not for θ=0° in the frequency range from 10 Hz to 10 kHz. Furthermore, the critical coincidence frequency decreases as the incident angle increases. However, the third observation for the last panel example is not applicable here. In fact, the trend is opposite for this example. That is, below the critical coincidence frequency f_c, the transmission loss is largest for ceramic-rich panel, while the metal-rich panel has lowest transmission loss below the critical coincidence frequency f_c. This indicates that the transmission loss depends on the specific material properties of an FGM panel, rather than on a simple relationship of metal–ceramic composition. Note that the results from the present study are consistent with those from different approach [14], supporting the accuracy of the present formulation.

4. Conclusions

In summary, we have developed an analytical solution for sound transmission and reflection for unbounded panels composed of functionally graded materials (FGM). We achieved this by following a procedure of variable re-grouping and matrix manipulation in converting the governing equations in the physical domain into the spectral domain. We were able to cast the governing equations with space-dependent coefficients into an equation system suitable for matrix integration,

thereby facilitating the derivation of the transfer matrix for an FGM panel. Our approach is unique in that FGM panels are treated as a single entity, and the effect of the gradation in material properties is automatically accounted for in the analytical formulation. This approach contrasts with the conventional treatment where the FGM panel is divided into multiple thin layers in order to seek a layer-wise analytical solution. Furthermore, our analytical solution includes multi-layer panels as a special case. In other words, our formulation treats both the multi-layer panel and FGM panel in a unified manner.

To verify the accuracy of the formulation, the analytical solution was applied to predict sound transmission loss for a single-layer isotropic panel and two metal–ceramic FGM panels. The results obtained were generally in good agreement with previously published data, either experimentally or numerically. Certain deviations may be caused by parameters that are not yet incorporated in the current study, such as the finite panel size, the panel mounting conditions at boundaries, and the acoustic damping of the panel materials. The effects of these parameters will be addressed in subsequent studies.

Several practical applications are related to the analytical formulations developed in this study. For example, the current formulation could be employed to study the sensitivity of sound transmission loss to various panel parameters. The parameter sensitivity would be useful to acoustic engineers to design and/or select panel materials to optimize sound transmission characteristics. A second application involves the design of panel layouts to meet specific acoustic requirements using given materials. In addition to such forward analysis and inverse design problems, there is yet another application that is related to system identification or material characterization for an FGM panel. In the FGM panel examples described, the distribution of metal or ceramic phase in the panel thickness direction was assumed to be known, as shown in Eqs. (55) and (56). In practice, this is rarely the case. In fact, it is often necessary to determine the phase distribution in an FGM panel by measuring the sound transmission. The analytical formulation of this study can be adjusted to undertake such material characterization tasks.

Acknowledgements

The authors are grateful for the financial support for this study from the Merwyn C. Gill Composites Center.

References

[1] H. Denli, J.Q. Sun, Structural–acoustic optimization of sandwich cylindrical shells for minimum interior sound transmission, *Journal of Sound and Vibration* 316 (2008) 32–49.
[2] R.G. Maev, *Acoustic Microscopy*, Wiley-VCH, Weinheim, 2008.
[3] S.R. Iyer, S.K. Sinha, A.J. Schokker, Ultrasonic C-scan imaging of post-tensioned concrete bridge structures for detection of corrosion and voids, *Computer-Aided Civil & Infrastructure Engineering* 20 (2005) 79–94.
[4] M. Meo, U. Polimeno, G. Zumpano, Detecting damage in composite materials using nonlinear elastic wave spectroscopy methods, *Applied Composite Materials* 15 (2008) 115–126.
[5] G.R. Liu, X. Han, K.Y. Lam, Stress wave in functionally gradient materials and its use for material characterization, *Composites Part B* 30 (1999) 383–394.
[6] G.R. Liu, X. Han, Y.G. Xu, K.Y. Lam, Materials characterization of functionally graded material by means of elastic waves and a progressive learning neural network, *Composites Science and Technology* 61 (2001) 1401–1411.
[7] G.R. Liu, J. Tani, Surface waves in functionally gradient piezoelectric material plates, *ASME Journal of Vibration and Acoustics* 116 (1994) 440–448.
[8] A. Chakraborty, S. Gopalakrishnan, Wave propagation in inhomogeneous layered media: solution of forward and inverse problems, *Acta Mechanica* 169 (2004) 153–185.
[9] J.N. Reddy, Analysis of functionally graded plates, *International Journal for Numerical Methods in Engineering* 47 (2000) 663–684.
[10] S. Venkataraman, B.V. Sankar, Elasticity solution for stresses in a sandwich beam with functionally graded core, *AIAA Journal* 41 (2003) 2501–2505.
[11] S.S. Vel, R.C. Batra, Exact solution for thermoelastic deformations of functionally graded thick rectangular plates, *AIAA Journal* 40 (2002) 1421–1433.
[12] L. Wang, S.I. Rokhlin, Recursive geometric integrators for wave propagation in a functionally graded multilayered elastic medium, *Journal of the Mechanics and Physics of Solids* 52 (2004) 2473–2506.
[13] A.L. Shuvalov, E.L. Clezio, G. Feuillard, The state-vector formalism and the Peano-series solution for modeling guided waves in functionally graded anisotropic piezoelectric plates, *International Journal of Engineering Science* 46 (2008) 929–947.
[14] S.M. Hasheminejad, M. Shabanimotlagh, Sound insulation characteristics of functionally graded panels, *Acta Acustica United with Acustica* 94 (2008) 290–300.
[15] W.T. Thomson, Transmission of elastic waves through a stratified solid medium, *Journal of Applied Physics* 21 (1950) 89–93.
[16] C.P. Smolenski, E.M. Krokosky, Dilational-mode sound transmission in sandwich panels, *Journal of the Acoustical Society of America* 54 (1973) 1449–1457.
[17] J.L. Guyader, C. Lesueur, Acoustic transmission through orthotropic multilayered plates, part II: transmission loss, *Journal of Sound and Vibration* 58 (1978) 69–86.
[18] C.L. Dym, D.C. Lang, Transmission loss of damped asymmetric sandwich panels with orthotropic cores, *Journal of Sound and Vibration* 88 (1983) 299–319.
[19] T. Wang, V.S. Sokolinsky, S. Rajaram, S.R. Nutt, Assessment of sandwich models for the prediction of sound transmission loss in unidirectional sandwich panels, *Applied Acoustics* 66 (2005) 245–262.
[20] S. Assaf, M. Guerich, Numerical prediction of noise transmission loss through visco-elastically damped sandwich plates, *Journal of Sandwich Structures and Materials* 10 (2008) 359–384.
[21] C. Cai, G.R. Liu, K.Y. Lam, An exact method for analyzing sound reflection and transmission by anisotropic laminates submerged in fluids, *Applied Acoustics* 61 (2000) 95–109.
[22] G.R. Liu, K.Y. Lam, Sound reflection and transmission of compliant plate-like structures by a plane sound wave excitation, *Journal of Sound and Vibration* 230 (2000) 809–824.
[23] H.J. Lin, C.N. Wang, Y.M. Kuo, Sound transmission loss across specially orthotropic laminates, *Applied Acoustics* 68 (2007) 1177–1191.
[24] C. Huang, S. Nutt, Sound transmission prediction using 3-D elasticity theory, *Journal of Applied Physics* 21 (2008) 89–93.

[25] F. Gilbert, G.A. Backus, Propagator matrices in elastic wave and vibration problems, *Geophysics* 31 (1966) 326–332.
[26] K. Aki, P.G. Richards, *Quantitative Seismology*, second ed., University Science Books, Sausalito, California, 2002.
[27] N.J. Higham, The scaling and squaring method for the matrix exponential revisited, *SIAM Journal on Matrix Analysis and Applications* 26 (2005) 1179–1193.
[28] G.R. Liu, *Elastic Waves in Anisotropic Laminates*, CRC Press, 2001.
[29] F.G. Leppington, K.H. Heron, E.G. Broadbent, F.R.S., S.M. Mead, Resonant and non-resonant acoustic properties of elastic panels. II. The transmission problem, *Proceedings of the Royal Society of London A* 412 (1987) 309–337.
[30] J. Wang, T.J. Lu, J. Woodhouse, R.S. Langley, J. Evans, Sound transmission through lightweight double-leaf partitions: theoretical modeling, *Journal of Sound and Vibration* 286 (2005) 817–847.
[31] M. Villot, C. Guigou, L. Gagliardini, Predicting the acoustical radiation of finite size multi-layered structures by applying spatial windowing on infinite structures, *Journal of Sound and Vibration* 245 (2001) 433–455.